



**LUT**  
Lappeenranta  
University of Technology

## **Power-to-X technology using renewable electricity and carbon dioxide from ambient air: SOLETAIR proof-of-concept and improved process concept**

Vidal Vázquez Francisco, Koponen Joonas, Ruuskanen Vesa, Bajamundi Cyril, Kosonen Antti, Simell Pekka, Ahola Jero, Frilund Christian, Elfving Jere, Reinikainen Matti, Heikkinen Niko, Kauppinen Juho, Piermartini Paolo

This is a Final draft version of a publication

published by Elsevier

in Journal of CO2 Utilization

**DOI:** 10.1016/j.jcou.2018.09.026

**Copyright of the original publication:** © 2018 Elsevier Ltd.

### **Please cite the publication as follows:**

Vidal Vázquez, F., Koponen, J., Ruuskanen, V., Bajamundi, C., Kosonen, A., Simell, P., Ahola, J., Frilund, C., Elfving, J., Reinikainen, M., Heikkinen, N., Kauppinen, J., Piermartini, P. (2018). Power-to-X technology using renewable electricity and carbon dioxide from ambient air: SOLETAIR proof-of-concept and improved process concept. *Journal of CO2 Utilization*, Vol 28, p. 235-246. DOI: 10.1016/j.jcou.2018.09.026

**This is a parallel published version of an original publication.  
This version can differ from the original published article.**

# Power-to-X Technology Using Renewable Electricity and Carbon Dioxide from Ambient Air: SOLETAIR Proof-of-Concept and Improved Process Concept

Francisco Vidal Vázquez<sup>a</sup>, Joonas Koponen<sup>b</sup>, Vesa Ruuskanen<sup>b</sup>, Cyril Bajamundi<sup>a</sup>, Antti Kosonen<sup>b</sup>, Pekka Simell<sup>a</sup>, Jero Ahola<sup>b</sup>, Christian Frilund<sup>a</sup>, Jere Elfving<sup>a</sup>, Matti Reinikainen<sup>a</sup>, Niko Heikkinen<sup>a</sup>, Juho Kauppinen<sup>a</sup>, Paolo Piermartini<sup>c</sup>

<sup>a</sup>*VTT Technical Research Centre of Finland Ltd, PL 1000, 02044 VTT, Finland*

<sup>b</sup>*Lappeenranta University of Technology, P.O. Box 20, 53851, Lappeenranta, Finland*

<sup>c</sup>*INERATEC GmbH Noerdliche Uferstr. 4-6, 76135, Karlsruhe, Germany*

---

## Abstract

This work demonstrates hydrocarbon production directly from water, solar energy, and air—called SOLETAIR. The plant includes direct air capture (DAC) of carbon dioxide, hydrogen production by water electrolysis, and two-step synthesis bench-scale units that operate using grid-connected solar photovoltaic (PV) electricity. In addition, co-feeding of hydrogen and carbon monoxide from gas bundles are utilized to enable scaling between units. This pilot plant achieved a total operating time of approx. 300 h with a combined production of oil and wax of 6.2 kg per day. The mass and energy balances in integration of the units are studied. According to the experiments and studies, potential and bottlenecks to improve the individual units and their integration are found. Finally, a conceptual Power-to-X plant is presented, which can achieve energy and carbon efficiencies of 47% and 94%, respectively, considering liquid and solid hydrocarbons as products.

*Keywords:* Power-to-X, carbon capture and utilization, direct air capture, water electrolysis, Firscher-Tropsch synthesis

---

## 1. Introduction

According to the Paris UN Climate Change Conference held in December 2015 [1], the CO<sub>2</sub> net emissions of the whole energy sector have to be close to zero by 2050 to limit the global mean temperature rise under 1.5°C above the preindustrial level. A change of this nature would require practically CO<sub>2</sub>-free power generation, and the energy system could thus be based predominantly on wind and solar power [2]. However, there are three main barriers to this transition: the intermittency of solar and wind power, the fuel needs of the transport sector, and the production of chemicals. Firstly, both solar and wind power are intermittent by nature, which generally leads to an imbalance between energy generation and consumption if no storage capacity is available. Secondly, the electrification of the whole transportation sector, such as passenger jets, cargo vessels, and heavy working machines, will present a major challenge. Instead, they can be electrified indirectly by using renewable hydrogen or hydrocarbons as their fuel, for example. Thirdly, the chemical industry sector is a significant consumer of oil and gas that are used as a feedstock for manufacturing e.g. plastics and nitrogen-based fertilizers, which should also be based on the use of renewables.

Fuels produced from CO<sub>2</sub> captured from ambient air can be carbon neutral as the cycle of CO<sub>2</sub> is closed [3, 4]. The potential global upper bound for annual CO<sub>2</sub> removal has been estimated to be in the scale of 10 Gt for direct air capture (DAC) with reliable storage [5]. When driven with renewable

energy, DAC is a net negative CO<sub>2</sub> emissions technology that can sequester previously emitted carbon dioxide from point and diffuse sources such as transportation [6]. Furthermore, there are already studies related to DAC technology that present select cases where the separation of CO<sub>2</sub> from the air to moderate purities is energetically equivalent to the work requirements using other CO<sub>2</sub> separation techniques from flue gases with high concentration of CO<sub>2</sub> [7, 8].

Power-to-Gas, Power-to-Liquids, or more generically, Power-to-X conversion concepts arise as a synergetic solution both for storing energy from intermittent renewable energy sources and producing carbon-neutral fuels from CO<sub>2</sub> emissions [9]. Piloting of the Power-to-X technologies is gaining ground and even reaching an industrial scale, the Audi methanation plant (synthetic natural gas production using alkaline water electrolysis and methanation of raw biogas), the Carbon Recycling International methanol synthesis plant (alkaline electrolysis, geothermal steam emission CO<sub>2</sub>, and methanol synthesis), and the Sunfire Power-to-Liquids plant (solid oxide electrolysis, DAC, and FT synthesis planned) being examples of this trend [10, 11, 12].

Many technologies can be applied for the production of fuels and chemicals from CO<sub>2</sub> and H<sub>2</sub>, such as synthetic natural gas, Fischer-Tropsch (FT) products, methanol, or even polymers and specialty chemicals. For the Power-to-X concept, these products are part of the few solutions existing for seasonal storage of energy. The production of kerosene or other heavy fuels from CO<sub>2</sub> emissions and renewable electricity is gaining interest to indirectly electrify aviation and heavy-duty transportation sectors. It has been estimated that the indirect electrification of the transportation sector would

increase the electricity consumption in the European Union from 2.8 PW h in 2013 to more than 10 PW h in 2050. Furthermore, the main part of electricity would be used for water electrolysis to produce hydrogen for Power-to-X processes [13, 14, 15].

In this paper, a Power-to-X process is experimentally verified with a modular and transportable pilot plant capable to produce renewable liquid and solid hydrocarbons. The mass and energy balances of the complete Power-to-X process are studied for the production of gaseous, liquid, and solid hydrocarbons from solar energy, water and CO<sub>2</sub> captured from ambient air. This is the first Power-to-X pilot plant in which the complete process chain is in the same place. Each of pilot plant's units—DAC, water electrolysis, and two-step synthesis—are experimentally studied. The experimental results, together with literature and process simulations, are then used as a basis for improving the entire system. Based on these improvements, a theoretical Power-to-X concept plant is presented where the developed process concept focuses on the energy and carbon efficiencies of the complete Power-to-X process.

## **2. Fundamentals of the Power-to-X process**

Renewable electricity from a solar PV power plant is used for DAC of CO<sub>2</sub>, hydrogen production with water electrolysis, and two-step synthesis process. CO<sub>2</sub> and hydrogen are supplied to FT process to produce gas, liquid and solid hydrocarbons as shown in Fig. 1. Fundamentals of each of the main units of the Power-to-X process are introduced in the following subsections.



Figure 1: The main idea of the SOLETAIR Power-to-X process producing CO<sub>2</sub> neutral hydrocarbons with renewable electricity.

### 2.1. Direct air capture of carbon dioxide

DAC is a technology for collecting CO<sub>2</sub> from ambient air, where the concentration of CO<sub>2</sub> is orders of magnitude lower than that of point sources such as flue gas and other industrial emissions. DAC uses a medium (solid or liquid) that has an affinity to CO<sub>2</sub>. *The medium is a base which forms covalent bond with the partially acidic C atom of CO<sub>2</sub> [16].* The most common medium for DAC is solid sorbents containing amines. These sorbents capture CO<sub>2</sub> by a chemisorption process *forming a carbamate ion or carbamic acid [17].*

To collect the chemisorbed CO<sub>2</sub> and regenerate the adsorbent, heat and/or vacuum is applied. When both heat and vacuum is used, the process is called temperature-vacuum swing adsorption (TVSA) process, which allows the operation of the desorption at a lower temperature ( $\leq 100^\circ\text{C}$ ) compared to temperature-swing adsorption. This is an attractive option since low-quality

heat can be used.

*Research on the improvement of DAC extensively involves the development of adsorbent properties to increase the CO<sub>2</sub> working capacity [18]. Amine bearing polymers such as polyethylenimine (PEI) impregnated to supports have been widely used as the active compound for CO<sub>2</sub> capture applications [19, 20, 21, 22, 23, 24]. Aminosilanes which are covalently bonded to supports have also been applied for DAC [25, 26, 27, 28, 29]. Metal organic frameworks have also been recently developed with reported capability to maintain working capacity even after exposure to humid air [30].*

*In addition to sorbent development, the adsorption chamber design and process control can be improved. First, the DAC systems require a significant amount of air to meet the production requirement because of the dilute concentration of CO<sub>2</sub>. Secondly, as DAC uses ambient air, the need to control the process based on weather conditions is equally important to optimize the energy consumption of the process.*

## *2.2. PEM water electrolysis*

In water electrolysis, electrical and thermal energy are converted into chemical energy, which is stored as hydrogen, and oxygen is produced as a byproduct. According to Faraday's laws of electrolysis, the production of hydrogen is directly proportional to the electric charge transferred at the electrodes. The lowest voltage required for the water decomposition to occur is called the reversible voltage. Without auxiliary heat, the minimum voltage required is higher than the reversible voltage, i.e. the thermoneutral voltage level [31, 32]. The reversible voltage and thermoneutral voltage at standard ambient conditions are 1.23 V and 1.48 V, respectively. According to the

thermoneutral voltage, the minimum energy required to produce one kg of hydrogen is 39.4 kWh, which is equal to the higher heating value (HHV) of hydrogen.

Polymer electrolyte membrane (PEM) water electrolysis has gained interest due to its compact system design, reportedly superior dynamic operation capability [13, 33, 34], and high voltage efficiency (<82% HHV) at greater current densities compared to the traditional alkaline technology. The high cost of components and typically inferior lifetime have been the main factors limiting the emergence of PEM technology [35], although improved stack power density and high efficiency have moved the technology into the MW-scale [36, 37]. Commercial PEM electrolyzers typically operate at current densities of  $0.6 \text{ A cm}^{-2}$ – $2.0 \text{ A cm}^{-2}$  and at operating temperatures of  $50 \text{ }^\circ\text{C}$ – $80 \text{ }^\circ\text{C}$ , while alkaline electrolyzers operate at current densities of  $0.2 \text{ A cm}^{-2}$ – $0.4 \text{ A cm}^{-2}$  [33]. The system cost for PEM water electrolyzers has been reported to be almost two times of the cost of traditional alkaline water electrolysis systems [34].

### *2.3. Two-step synthesis*

FT is a well-known technology for production of gas, liquid, and solid hydrocarbons from synthesis gas, also named syngas. Syngas contains a mixture of  $\text{H}_2$  and  $\text{CO}$ , and usually some  $\text{CO}_2$ . The product consists of a distribution of linear hydrocarbons of different carbon numbers, which obey the Anderson-Schulz-Flory (ASF) distribution [38]. The ASF distribution can be described using one parameter, the chain-growth probability ( $\alpha$ ). The product distribution depends on the operating conditions and the catalyst composition. FT is a highly exothermic reaction operated at high pressures

(20 bar–30 bar) and relatively low temperatures (180 °C–250 °C). FT catalysts perform with low activity (Fe-based catalysts) or complete inactivity (Co-based catalysts) towards CO<sub>2</sub>. Thus, CO-rich syngas is required as a feedstock of the FT. For that reason, using CO<sub>2</sub> as a carbon source requires a two-step process combining production of CO from CO<sub>2</sub> by reverse Water-Gas Shift (rWGS) reaction and subsequent FT [39].

The rWGS is an endothermic reaction favorable at high temperatures (over 600 °C). The chemical equilibrium of rWGS is independent on pressure, and product formation increases with increasing temperature. However, operating rWGS at a high pressure has its advantages and disadvantages. High pressure increases methane formation by methanation reactions, and even carbon formation by the Boudouard reaction or other carbon formation reactions. On the other hand, operating at a high pressure reduces the reactor size by increasing the residence time of the reactants in the reactor and provides an option of removing compression between the rWGS and the FT if both steps are operated at the same pressure [40, 41].

### **3. Description of the SOLETAIR pilot plant**

The pilot plant was located at the premises of Lappeenranta University of Technology (LUT) in the summer of 2017. The pilot plant consisted of four parts; a 206.5 kW<sub>p</sub> solar PV power plant [42], a DAC unit, a hydrogen production unit [43], and a two-step synthesis unit. However, the production capacities for H<sub>2</sub> and DAC were lower than the feed requirement of the synthesis unit. For that reason, a gas container was used for co-feeding of CO and H<sub>2</sub>. Furthermore, electricity from the grid was used to run the elec-

trolysis in the night-time as no electric battery unit was integrated into the system—the carbon intensity of grid electricity in Finland is  $0.2 \text{ kgkWh}^{-1}$  [44]. Technical specifications of the pilot plant are presented in Table 1. The key sea-container-installation units of the pilot plant (DAC, hydrogen production, and mobile synthesis) are illustrated in Fig. 2.

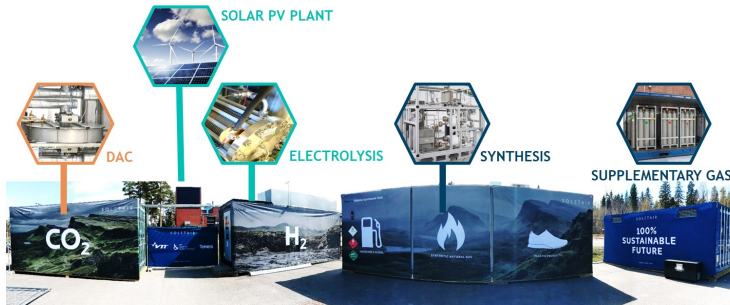


Figure 2: SOLETAIR pilot site.

Table 1: Technical specifications of the DAC unit, electrolysis unit, and the two-step synthesis unit with the most relevant values.

DAC unit		Water electrolysis unit		Two-step synthesis unit	
Rated CO <sub>2</sub> production	3800 g d <sup>-1</sup>	Hydrogen production rate	90 g h <sup>-1</sup>	Preheater rWGS temp.	max. 450 °C
<i>Max. air flow</i>	1500 m <sup>3</sup> h <sup>-1</sup>	Nominal stack power	4.5 kW	rWGS temp.	850 °C
<i>Air temp. for blowers</i>	-40 °C-80 °C	Nominal voltage	64 V	rWGS pressure	1 bar-5 bar
Vacuum (desorption, min)	5 mbar	Nominal current	70 A	Condenser rWGS temp.	0 °C-5 °C
<i>Max. water temp.</i>	100 °C	Operating temp.	70 °C	Compression ratio	5-10
Cartridge content	<i>Amine-funct. polymer resin</i>	Number of cells in series	33	Preheater FT	200 °C
Number of cartridge/bed	8	Cell cross-sectional area	69 cm <sup>2</sup>	FT temp.	200 °C-250 °C
Mass of adsorbent/cartridge	30 kg	Hydrogen purity	>99.995%	FT pressure	20 bar-30 bar
<i>Temp. of operation</i>	ambient to 90 °C	Hydrogen pressure	15 bar-50 bar	Hot trap temp.	165 °C-170 °C
Pressure (adsorption)	1.005 bar	Oxygen pressure	1.5 bar-2.5 bar	Cold trap temp.	5 °C-10 °C

### 3.1. Direct air capture unit

Key specifications of the DAC unit used in this study are listed in Table 1. Characterization and equilibrium performance of the adsorbent are presented

in [45, 46]. The DAC unit (developed and supplied by Hydrocell Oy) was instrumented for data collection, visualization, and analysis.

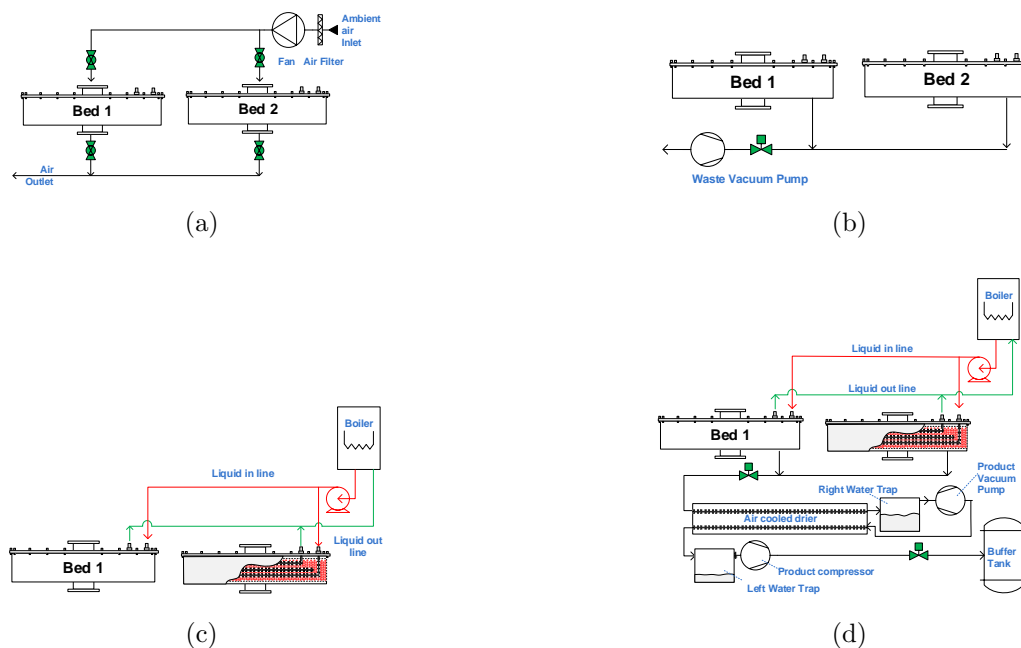


Figure 3: Stages of TVSA operation of the DAC unit. (a) Adsorption. (b) Purging. (c) Heating. (d) Desorption.

The operating principle of the DAC is shown in Fig. 3. Immersed in the bed of adsorbent is a brush type heat exchanger, which is used to heat the bed during the desorption step. Two beds are operated in parallel, and they are subject to the same stage of operation simultaneously. There are four stages of the TVSA operation. The first stage of operation is the adsorption process (Fig. 3a) that lasts for ca. 20 h. In this stage, air is led through the column via a flow distribution plate to maximize mass transfer. In the second stage (Fig. 3b), the remaining air (mainly  $O_2$  and  $N_2$ ) is removed using a two-stage vacuum pump. The purging step is essential to achieve high-purity  $CO_2$

gas required for the synthesis. Purging lasts for 15 min. The next stage in the operation is the heating stage, and it lasts for 30 min (Fig. 3c). Warm glycol-water mixture (20% ethylene glycol) from a 3 kW boiler is pumped to the intra-bed heat exchanger to preheat the bed and desorb some gases in preparation for the next step, shown in Fig. 3d. Finally, after the preheating stage, CO<sub>2</sub> is collected from the bed through the product gas line. The hot gases from the beds pass through an ambient-air-cooled heat exchanger and a water trap (right water trap) before being sucked by the product vacuum pump. Then, the product gas, which is mainly CO<sub>2</sub> at this point, passes again through the ambient-air-cooled heat exchanger and another water trap (left water trap) for further cooling and drying before being compressed. The product gas is stored in a gas bundle (12 × 50 L) and a 50 L buffer tank.

### *3.2. Hydrogen production unit*

A hydrogen laboratory system manufactured by IRD Fuel Cells (currently known as EWII Fuel Cells) is built in a standard shipping container. The hydrogen production process in the laboratory setup is the following: Inlet water to the electrolyzer is first deionized to decrease the conductivity of the supplied water. The commercial PEM water electrolyzer E1050 (IRD) system, which is illustrated in Fig. 4 and presented according to its technical specifications in Table 1, then decomposes the water into hydrogen and oxygen. The water electrolyzer is powered by two PAP3200 DC power supplies (Powerfinn) connected in parallel. The dew point of the outlet hydrogen gas is then decreased in a hydrogen gas drying unit (IRD) to  $-70^{\circ}\text{C}$  to prepare it for outdoor storage in Nordic conditions. The total volume of the pressurized hydrogen gas storage is 700 L. Both the hydrogen and oxygen gas outlet

pressures are controlled by back-pressure valves. The designed pressure levels of the E1050 electrolyzer for hydrogen and oxygen gases are 50 bar and 2 bar, respectively.

Operating temperature, water inlet pressure, water conductivity and flow, hydrogen outlet pressure, stack voltage, stack current and individual cell voltages are measured by the IRD’s measurement system. An additional data acquisition system (National Instruments) was added to support the existing monitoring system.

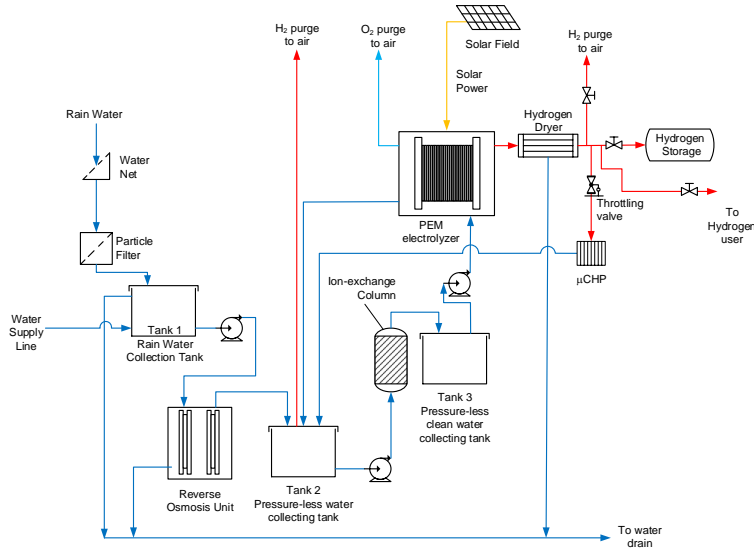


Figure 4: Simplified process flow diagram of the H<sub>2</sub> production system.

### 3.3. Mobile synthesis unit for the two-step process

The mobile synthesis unit is a multi-purpose container-size demonstration unit. The two-step process, illustrated in Fig. 5, consists of a rWGS module (VTT) and a FT micro-structured heat exchanger reactor (INERATEC). A summary of the specifications of this setup are presented in Table 1.

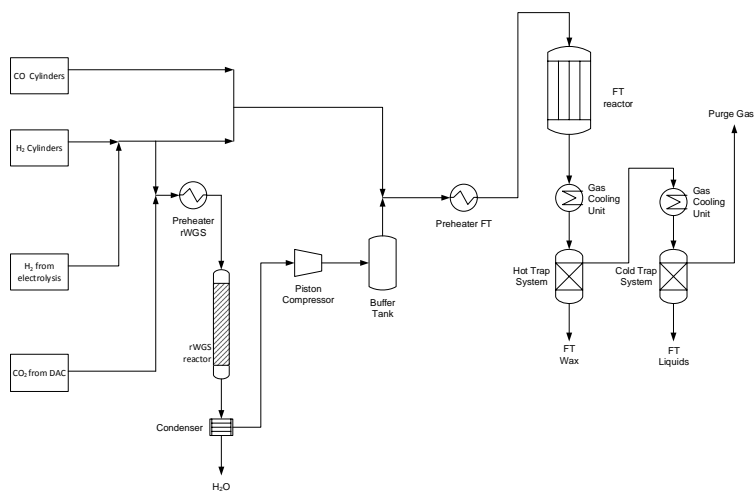


Figure 5: Simplified process flow diagram of the mobile synthesis unit.

The rWGS reaction is performed in a fire-proof steel tubular reactor filled with metallic monoliths of 20 mm in diameter coated with precious metal catalyst. The reactor is dimensioned for CO<sub>2</sub> inlet flow rate of 2 N L min<sup>-1</sup> based on the maximum CO<sub>2</sub> production capacity of the DAC unit. The tubular reactor is heated externally by an electric oven. The gas mixture is externally electrically preheated to temperatures up to 450 °C before entering the reactor. Two thermocouples are placed at the top and bottom of the catalyst bed. The reactor could be operated at a maximum of 850 °C and 10 bar due to the limitations of the construction material of the reactor. The reactor operating conditions are kept constant during the test campaigns at 850 °C at the outlet of the catalyst bed, and 4 bar pressure. The feed gas for the rWGS is 0.6 L min<sup>-1</sup>–0.8 L min<sup>-1</sup> of CO<sub>2</sub>, 1.2 L min<sup>-1</sup>–1.6 L min<sup>-1</sup> of H<sub>2</sub> and 0.11 L min<sup>-1</sup>–0.15 L min<sup>-1</sup> of N<sub>2</sub>. Nitrogen is added for gas analysis purposes. The feed gas composition for the rWGS is adjusted to produce

an outlet gas composition of the rWGS with a  $\text{H}_2/\text{CO}$  ratio  $\approx 2.1$  matching the requirements of the FT process. The gas feedstock for rWGS was kept constant during the test campaign as long as possible. An air-driven piston compressor compresses the syngas produced by the rWGS from 4 bar to over 20 bar (operating pressure of the FT reactor).

The FT is performed using an industrial cobalt-based catalyst in a plate-type microstructured heat exchanger reactor cooled by high-pressure boiling water. The reactor is dimensioned for inlet flow rates up to  $2 \text{ Nm}^3\text{h}^{-1}$  of CO and  $4 \text{ Nm}^3\text{h}^{-1}$  of  $\text{H}_2$ . However, FT module employs only  $1 \text{ Nm}^3\text{h}^{-1}$  of CO and  $2 \text{ Nm}^3\text{h}^{-1}$  of  $\text{H}_2$  for the test campaigns of this work. Owing to the limitations of the  $\text{CO}_2$  production from the DAC unit and  $\text{H}_2$  production from the PEM electrolysis unit, the FT module requires co-feeding of stored bundles of both CO and  $\text{H}_2$  to match the continuous feed requirements ( $1 \text{ Nm}^3\text{h}_{\text{CO}}^{-1}$  and  $2 \text{ Nm}^3\text{h}_{\text{H}_2}^{-1}$ ). These bundle gases of CO and  $\text{H}_2$  (AGA) have a gas quality of 99.8% and 99.95%, respectively. The FT reactor is operated at  $230\text{ }^\circ\text{C}$ – $240\text{ }^\circ\text{C}$  and ca. 20 bar. After the FT reactor, the products are separated by condensation at different temperatures (Fig. 5). First, the solid product is condensed in a hot trap at a temperature around  $165\text{ }^\circ\text{C}$ – $170\text{ }^\circ\text{C}$ . Then, the liquid product is condensed in a cold trap at a temperature of  $5\text{ }^\circ\text{C}$ – $10\text{ }^\circ\text{C}$ . This liquid product is formed by an aqueous phase and an oil phase. The rest of FT products and unreacted gases are vented into the atmosphere during the tests. Part of this gas is used for online analysis purposes. The conversion of the reactants and the FT gas product composition are calculated using an online gas chromatograph. The composition of the solid and liquid products are analyzed a posteriori by gas chromatography. The liquid product is

analyzed as such while the solid product is dissolved in cyclohexane.

## 4. Results and discussion

### 4.1. Experimental results

The test campaigns of this study were performed in summer during weeks 24, 26, 28, and 32 of 2017. The FT process was set to emphasize wax production for demonstration purposes. The units were operated simultaneously during these four test campaigns. The exact duration of the test campaigns varied as explained in the following subsections. The main objective of these test campaigns was proving the concept and gaining operational experience by running the system continuously during the test week. Further, the overall operation and energy balance of the bench-scale plant are analyzed.

#### 4.1.1. CO<sub>2</sub> capture from air

Adsorption began immediately after the desorption period of the previous cycle, which is illustrated in Fig. 6. Introducing ambient air (400 ppm with very minor variations in concentration) to the hot bed increases the CO<sub>2</sub> concentration, temperature and humidity of the air leaving the beds. After about 1 h, the CO<sub>2</sub> concentration at the inlet and outlet were equal, which signified the actual start of CO<sub>2</sub> adsorption. During the first three hours of the adsorption, the CO<sub>2</sub> concentration of the exiting air could decrease as low as 100 ppm for all the beds. As the adsorption continued, the CO<sub>2</sub> concentration at the exit started to increase and approached the inlet concentration indicating saturation of the bed. During the adsorption process, the pressure drop across the bed is 400 mbar. At the start of the heating

process, warm liquid entered the intra-bed heat exchanger at around 80 °C and left at 55 °C. The bed was at ambient temperature. At the start of the desorption period, the bed and the liquid leaving the bed were almost at the same temperature and were rising at a rate of 0.25 °C min<sup>-1</sup> until the inlet temperature reached about 90 °C. The 90 °C limit was set to protect the adsorbents from excessive heating, which may degrade the material. Thirty minutes before the desorption ended, the temperature of the bed and the liquid inlet/outlet point dropped abruptly as a result of heating the next bed pairs. The desorbing beds are in parallel with the beds being heated. The heating power of the boiler is shared between the two bed sets. At the end of the desorption, the bed temperature rapidly cooled down as a result of blowing cooler ambient air directly to the bed.



Figure 6: CO<sub>2</sub> and temperature at the inlet and outlet of beds 3 and 4. (a) CO<sub>2</sub> concentration. (b) Temperature.

Fig. 7 also shows the waste and product vacuum line pressure in the production phase. During the purging step, the bed was closed and waste gases were removed by vacuuming down to 50 mbar(abs). The bed vacuum pressure is presented as the product vacuum line. The purging step was performed isothermally and thus, only pressure was changed. As reported



Figure 7: Key temperature and vacuum pressure measured for Bed 4 during the production phase.  $r$  is the radial distance from the center of the bed. The radius of a bed is 500 mm. (a) Temperature. (b) Vacuum pressure.

elsewhere, the effect of pressure in the desorption of  $\text{CO}_2$  is much less significant than the effect of temperature [45]. For this reason, the loss of  $\text{CO}_2$  during the purging step was considered insignificant. Over the desorption period, the vacuum pressure was between 100 mbar(abs) and 200 mbar(abs). The current setup could not maintain an isobaric condition during the vacuum operation because of problems in the product gas compressor operation. As a result, there was significant variation in the amount of  $\text{CO}_2$  and water produced (see Table 2). From the production data, the mean molar ratio of  $\text{H}_2\text{O}:\text{CO}_2$  was 4.6. The quality of DAC produced water is compared to the deionized water supplied to the PEM water electrolyzer in Table 3.

The  $\text{CO}_2$  gas quality during the test campaign is given in Table 2. The medians of  $\text{CO}_2$  concentrations were all above 97 vol-% in all test campaigns. The equilibrium working capacity of the adsorbent (moles of  $\text{CO}_2$  per kilogram of adsorbent) is reported elsewhere [45]. Due to the large variation in  $\text{CO}_2$  production in this device, it is difficult to provide a meaningful comparison between the equilibrium working capacity reported in [45]. In a test

Table 2: Daily production data, energy usage, and product gas quality of the DAC during the SOLETAIR campaign periods. Some test days were excluded from the analysis due to missing data when the logging system was not running.

Stat.	CO <sub>2</sub> prod.	H <sub>2</sub> O prod.	$E_{\text{used}}$	$E_{\text{specific}}$	CO <sub>2</sub>	H <sub>2</sub> O	O <sub>2</sub>
(-)	(g)	(g)	(kWh)	(kWhkg <sup>-1</sup> <sub>CO<sub>2</sub></sub> )	(vol-%)	(vol-%)	(vol-%)
min	729	1493	27.5	15.0	93.85	0.12	0
max	2749	4770	41.8	49.0	100	1.17	1.59
mean, $\mu$	1564	2954	36.9	26.4	98.55	0.58	0.3
std. dev., $\sigma$	549	939	4.4	10.5	0.70	0.23	0.23
$\sigma/\mu$	0.35	0.32	0.12	0.40	0.007	0.40	0.74

Table 3: Quality of the water from the DAC and the water fed to the electrolyzer.

Sample	Total carbon	Total nitrogen	NH <sub>4</sub>	pH	Conductivity
	(mg L <sup>-1</sup> )	(mg L <sup>-1</sup> )	(mg L <sup>-1</sup> )	(-)	( $\mu\text{S cm}^{-1}$ )
DAC water	119	101	113.7	7.59	679.5
Electrolysis water	6	0	<0.05	5.27	2.222

campaign, the collected CO<sub>2</sub> gas was fed straight to the rWGS reactor of the two-step synthesis process without further purification.

The power consumption of the DAC had two distinct regions. The low power usage region, which lasted for ca. 15 h with a power usage of 0.6 kW, occurred when the fans were the only power-consuming devices during the adsorption period. Then, the high power usage region, which lasted for approx. 9 h with an average power usage of 4 kW, occurred for the desorption period when the boiler was running and was consuming most of the power.

The total energy used per cycle is calculated from power data. Unlike the CO<sub>2</sub> production, the energy used per cycle does not vary significantly (see Table 2) because the operation schedule is almost constant for all the test

runs. There were instances during the production operation when the boiler temperature had reached 90 °C and caused the boiler to turn off for about 30 min; this caused the variability in total energy consumption of the cycle.

The electrical requirement is for driving the fans, vacuuming, product compression, data logging setup, and heating the liquid pump. On average, 57.8% of the specific energy requirement is for the thermal requirement, the rest is for the electrical requirement. The average total energy consumption is  $26.4 \text{ kWhkg}_{\text{CO}_2}^{-1}$ , which is an order of magnitude higher compared to the energy requirements of Climeworks DAC unit. Climeworks state an energy requirement of  $1.8 \text{ kWhkg}_{\text{CO}_2}^{-1}$ – $2.45 \text{ kWhkg}_{\text{CO}_2}^{-1}$  (data obtained by request through Climeworks webpage [47]). However, if the amount of  $\text{CO}_2$  reaches the designed production capacity of 3.8 kg/cycle by improving the mechanical components of the DAC, the specific energy requirement can be lowered to  $9.7 \text{ kWh kg}^{-1}$  (based on the mean energy used in Table 2). The production levels of this DAC compared to Climeworks are orders of magnitude different. The high energy requirements of the experimental results was attributed to the losses generated by the relatively small system of the DAC unit where heat losses and compression and vacuum power become very significant.

#### *4.1.2. Hydrogen production*

The PEM water electrolysis system presented in Section 3 is smaller in hydrogen production capacity than the FT synthesis in terms of hydrogen consumption. Therefore, the PEM water electrolyser was set to operate at its nominal production capacity of  $1 \text{ Nm}^3\text{h}^{-1}$  ( $90 \text{ g h}^{-1}$ ) throughout the test campaigns. Partial load operation was not considered, since hydrogen production had to be maximized. The hydrogen stack outlet pressure was

controlled down to 40 bar, while the pressure level in the synthesis process was controlled to 20 bar. The designed hydrogen stack outlet pressure of 50 bar was not selected to ensure continuous operation. The higher pressure from the water electrolyser ensured that the hydrogen production could operate continuously even if the synthesis process would stop for an extended period of time, as the PEM water electrolyzer is set to automatically shut down if the storage pressure meets the hydrogen stack outlet pressure. The oxygen stack outlet pressure was controlled to the nominal 2 bar. The water electrolyser stack was water cooled to 71 °C.

The continuous run times and key mean measurement results from the PEM water electrolysis system are presented in Table 4. The mean stack voltage increases from 60.26 V to 60.63 V over the test campaign weeks. The stack voltage increase can be explained by the increasing trend of the inlet water conductivity. The average stack specific energy consumption was  $49 \text{ kWhkg}_{\text{H}_2}^{-1}$  assuming unity Faraday efficiency. However, if Faraday efficiency is considered, the stack specific energy consumption increases further. The Faraday efficiency of the studied PEM water electrolyzer at 40 bar has been identified as  $\geq 95\%$  in nominal operation in [43]. With an assumed Faraday efficiency of 95%, the stack specific energy consumption increases from  $49 \text{ kWhkg}_{\text{H}_2}^{-1}$  to  $51 \text{ kWhkg}_{\text{H}_2}^{-1}$ . Additional losses in the hydrogen production system are caused by the hydrogen gas drying unit (average  $2.1 \text{ kWhkg}_{\text{H}_2}^{-1}$  in nominal operation) and the small-scale DC power supplies of the PEM water electrolyzer.

The energy needed for the water electrolysis is mainly consumed by the PEM stack converting around 80% of the supplied electrical energy into the

Table 4: Continuous system runtime and mean values of stack voltage, stack current, and stack inlet water conductivity as well as the produced hydrogen, stack energy consumption, and stack specific energy consumption from the hydrogen production system for each test campaign week. H<sub>2</sub> outlet pressure was controlled to 40 bar, O<sub>2</sub> outlet pressure to 2 bar, and stack temperature to 71 °C in all test campaigns.

Week	$t$	$U_{\text{stack}}$	$I_{\text{stack}}$	$\sigma$	H <sub>2</sub> prod.	$E_{\text{stack}}$	$E_{\text{s,stack}}$
(-)	(h)	(V)	(A)	( $\mu\text{S cm}^{-1}$ )	(kg)	(kW h)	( $\text{kWhkg}_{\text{H}_2}^{-1}$ )
24	72.72	60.26	70.20	1.98	6.31	307.6	48.8
26	95.13	60.39	70.23	2.04	8.25	403.5	48.9
28	100.72	60.53	70.21	2.37	8.74	428.0	49
32	94.00	60.63	70.23	3.12	8.16	400.4	49.1

chemical energy of the hydrogen gas. In the studied system, the efficiency of the DC power source supplying the electrolyzer stack is only around 90%, but the rectifiers used on the industrial scale may reach an efficiency higher than 97%.

#### 4.1.3. Two-step synthesis

The performance of the rWGS reactor was checked every test campaign. The temperature at the bottom of the catalyst bed and pressure of the reactor remained constant during operation with values of 808 °C and 4 bar. The CO<sub>2</sub> and H<sub>2</sub> conversions also remained unchanged throughout steady operation with values of 63 % and 34 %, respectively. The products were mainly CO and H<sub>2</sub>O, but some methane was formed as a side product. The yields of CO and CH<sub>4</sub> were 61.7 % and 1.3 %, respectively.

The performance of the FT reactor was continuously measured during each of the test campaigns. Fig. 8a shows the CO conversion over time of

each of the campaigns from the start of the campaign. The  $\text{H}_2$  conversion was always slightly lower compared to CO conversion due to the slightly over stoichiometric composition of the gas feedstock of the FT reactor with  $\text{H}_2/\text{CO}$  ratio of ca. 2.1. This over stoichiometric composition was chosen in order to avoid carbon formation in the FT reactor. For instance,  $\text{H}_2$  conversion was 58.5 % when CO conversion was 60.3 %. These conversion values were quite representative of the FT process performance [48]. Using these values, the overall  $\text{CO}_2$  and  $\text{H}_2$  conversions after the rWGS and FT steps were 38% and 72.6%, respectively. Nevertheless, Fig. 8a shows a decline in the catalytic activity of the FT catalyst, which seemed to stabilize after long periods of operation. This initial loss of activity was attributed to the increasing mass transfer limitations on the catalyst surface resulting from the formation and accumulation of the heavier fraction of the FT products in the reactor.

The rate of product formation also decreased over time for all the products as a consequence of the decrease in the CO conversion. However, the ratio between wax and oil formation rate increased over time. This indicated an increase in the average molecular weight of the products from the FT reactor, and thus, an increase in the average alpha value of the product distribution. This effect could be due to the accumulation of waxes in the reactor at the beginning of operation that stabilizes over time.

Fig. 8b shows the molar fraction of each component taking into account its amount in the oil and wax product. This chart also shows the slopes of the ASF distributions for alpha values of 0.875 and 0.935. The slope of the FT product with a lower carbon number ( $<C_{27}$ ) resembles to the ASF distribution where alpha is 0.875. However, the slope of the distribution

switches at values  $C_{27}$ – $C_{30}$ . The  $C_{30+}$  distribution resembles to an ASF distribution with an alpha value equal to 0.935. This kind of deviation of a product distribution combining two different alpha values has also been observed in the literature [38, 49]. The oil product contained hydrocarbons ranging mainly from  $C_4$  to  $C_{14}$  (91.1 mass-%). However, it also contained a small amount of propane (1.5 mass-%) and quite a significant amount of  $C_{15+}$  (7.4 mass-%). This analysis clearly showed that the oil phase easily dissolved propane and butane, which otherwise should be gas in ambient conditions. The oil product contained mainly paraffinic hydrocarbons but also small quantities of  $\alpha$ -olefins and alcohols. The wax product contained an even wider range of hydrocarbons from  $C_{11}$  to  $C_{38}$  (84.8 mass-%). It also contained  $<C_{11}$  (2.5 mass-%) and a significant amount of  $C_{39+}$  (12.7 mass-%). The wax product was also mainly formed of paraffinic hydrocarbons with traces of olefins. Further, the aqueous phase produced in the FT reactor contained significant amounts of linear alcohols with a chain length up to octanol. Thus, this aqueous phase would require purification before reuse in the system or to be released into the environment.

#### 4.1.4. Overall results

Fig. 9 shows the simplified diagram of the SOLETAIR pilot plant with the most relevant energy and material input and output streams for each unit during the first day of production on week 32. In the case of the two-step synthesis unit, the value of the electric power input was estimated based on the heat duty of the feed gas heaters and the rWGS reactor, and the duty of the compressor (Fig. 5). The duty of the piston compressor was calculated using an isentropic efficiency of 0.85 [50]. The two heat outputs correspond

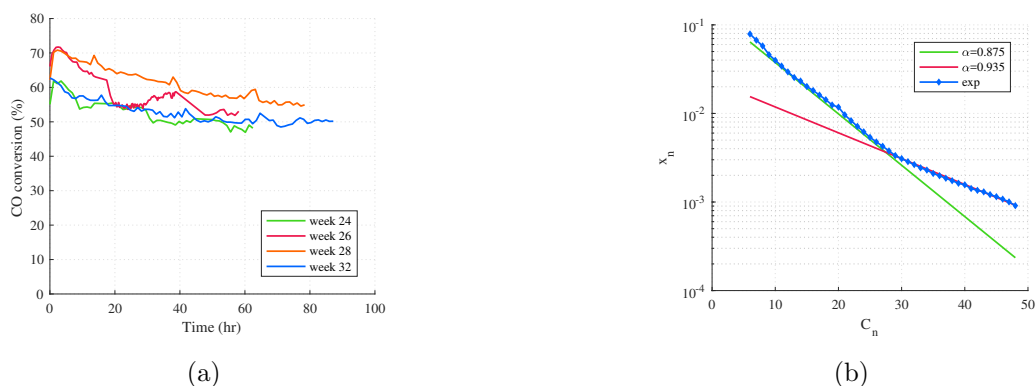


Figure 8: Measurements of FT synthesis. (a) CO conversion over time for each test campaign. (b) Molar fraction of the components contained in the sum of oil and wax products, and ASF distributions.

to the heat of the reaction from the FT reactor, and the rest of heat sources, which are the condenser and the gas cooling units. All the heat duties and the compressor duty were calculated by simulation in Aspen Plus.

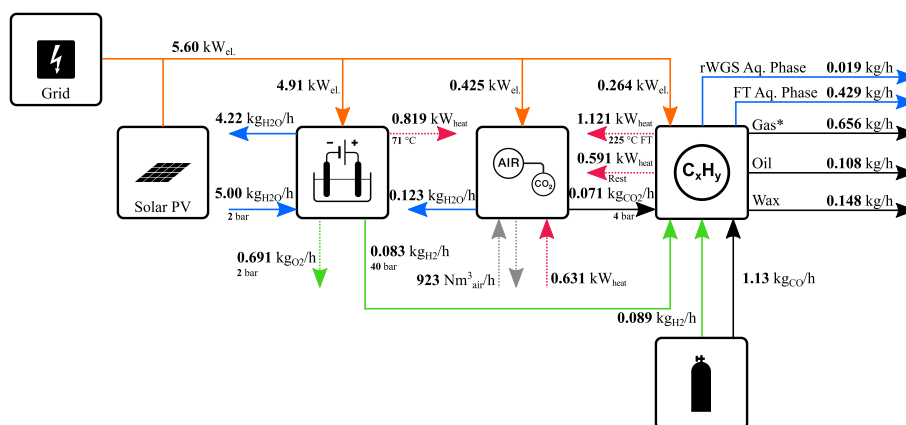


Figure 9: *Simplified diagram of the SOLETAIR pilot plant including mass and energy flow streams based on production during the first day of operation on week 32. \*Gas containing both the FT gas product and unreacted  $H_2$ ,  $CO$ , and  $CO_2$ .*

In the SOLETAIR pilot plant, only 30.8% of the hydrogen is bound into

the end products (including FT gas). Most of the hydrogen forms water together with oxygen in the rWGS and the FT. Moreover, a significant part of the hydrogen travels non-reacting through the synthesis process owing to the conversion limitation of each step of the two-step process. This also affects the energy efficiency of the process as hydrogen is the main energy carrier. 59.5% of the carbon ends up in the FT products. This carbon conversion number reduces to 38% when only the carbon contained in the CO<sub>2</sub> from the DAC is considered. The carbon efficiency is equal to the overall CO<sub>2</sub> conversion of the two-step synthesis by rWGS and FT. This is also due to the conversion limitation of the two-step process. A significant loss in the process is the chemical energy contained in the vented gases containing unreacted H<sub>2</sub> and CO, and FT gases. Therefore, recirculation of unreacted gases into the process is essential in increasing the overall carbon utilization.

#### *4.2. Theoretical Power-to-X plant*

The pilot plant described in Section 3 was far from optimal for several reasons. First, the process inside each unit was not optimized, and there was room for improvement in all units. The overall efficiency of the process could also be improved by integrating energy and mass flows between the units. Second, there was a clear mismatch of production capacities between the units because they were not sized only for the purposes of this study. Finally, these container-sized units constituted a relatively small-scale system. Therefore, the heat losses and peripheral equipment generated significant energy loss compared with the overall energy balance. For these reasons, a study of an improved Power-to-X plant was required to get a clear picture of its potential and limitations. The process concept development addressed

the issues of the Power-to-X pilot plant and aimed at maximizing the carbon and energy efficiency of each unit and the overall Power-to-X process during continuous operation.

#### *4.2.1. System improvement*

Several improvements have been made to this theoretical configuration over the SOLETAIR Power-to-X pilot plant. The improvements for DAC and water electrolysis are based both on experimental results and literature. In the case of the two-step synthesis, the improvements are also supported with simulations of an enhanced two-step synthesis process *using the Aspen Plus software*.

*The limitations in CO<sub>2</sub> and CO conversions can be overcome by recirculation of unreacted gases back to the first step of the two-step synthesis process. However, the gas effluent from product condensation after the FT reactor contains a significant amount of light hydrocarbons that have to be decomposed to form H<sub>2</sub> and CO again, as well as unreacted CO<sub>2</sub>, CO, and H<sub>2</sub>. Furthermore, these light hydrocarbons are more prone to form carbon at high temperatures than CO<sub>2</sub> and CO. This carbon can cause problems of fouling and clogging in the reactor. One solution for this problem is the catalytic partial oxidation (CPO) by addition of oxygen to the mixture of recirculated gas and fresh H<sub>2</sub> and CO<sub>2</sub> feed. The addition of oxygen together with the make-up gas and recirculation gas will help in decomposing the light hydrocarbons and avoiding carbon formation by increasing the O/C ratio in the feedstock of the first step of the process. Now, this first step is called the rWGS/CPO step because it includes both the rWGS reaction and CPO reactions of light hydrocarbons. However, pure O<sub>2</sub> has to be used in order to avoid dilution of*

*the gas mixture with inert components such as the  $N_2$  contained in the air. Thus, the  $O_2$  effluent from water electrolysis is a potential source of pure  $O_2$  for the new two-step process. However, most of the generated electrolytic oxygen would be unused and vented to the atmosphere or used for other external processes.*

*Another limitation of the two-step synthesis process is the compression between the two steps of the process. Hydrogen can be generated at a high pressure by the PEM electrolyzer (up to 50 bar). In the experimental setup, the pressure of the hydrogen was reduced to 4 bar in the rWGS step. Then, the syngas mixture after the rWGS reactor was compressed to the FT operating pressure (20 bar). Thus, operating the rWGS/CPO reactor at the same pressure as the FT reactor can save the energy used for compression of the syngas between the two steps. Temperature of the rWGS/CPO reactor also has to be increased in order to minimize the formation of methane, which is thermodynamically unfavorable at high temperatures.*

Furthermore, the DAC uses the excess heat of the synthesis unit and the water electrolysis. The DAC uses all of the heat from the synthesis unit that is above 80 °C, and part of the heat generated by the PEM stack to cover the heat requirement of the DAC process. However, 79% of the PEM stack excess heat remains unused, and it could be used for other processes that require low temperature heat. On the other hand, the electrolyzer excess heat could also be used for DAC if the higher temperature heat from the synthesis can be used in external processes. This exchange of thermal energy provides versatility depending on the location of the Power-to-X plant.

The water consumption of the electrolyzer could be further reduced by

utilizing the water collected in the DAC and the FT, albeit with some limitations. The water collected after the rWGS/CPO step is used to co-feed the electrolyzer to reduce its water consumption. Therefore, 10% of the water requirement for the hydrogen production unit is covered by water recirculation. The amount of water captured by the DAC is heavily dependent on the ambient conditions of humidity. However, the water captured by DAC should be further analyzed to understand the required water purification steps before PEM water electrolysis. Direct use of the DAC water is not reasonable due to the impurities as presented in Table 3. The FT aqueous phase includes significant amount of alcohols in its composition that range from methanol to octanol. These alcohols could accelerate the degradation of the PEM electrolyzer cells, and thus, these should be cleaned out.

#### *4.2.2. Results*

The theoretical Power-to-X plant is sized for a PEM electrolyzer stack of 1 MW. This process concept maximizes the overall carbon and energy efficiencies of the system. Special attention is paid to the use of excess heat and water supply between the units. The energy consumption of peripheral equipment (including civil and industrial areas) of the plant such as control systems or other instrumentation is neglected in the calculations.

Fig. 10 shows a simplified diagram of the theoretical Power-to-X plant sized for a PEM electrolyzer stack of 1 MW. This diagram shows the connections of the energy and material streams between units. A summary of the main technical specifications for each unit of the theoretical Power-to-X plant are presented in Table 5.

Fig. 11 presents the Sankey diagrams for the energy and mass balances

of the theoretical Power-to-X plant. As can be seen in Fig. 11b, 95% of the carbon supplied by the DAC ends up as FT products including gases. *The carbon efficiency is calculated from*

$$\eta_C = \frac{m_{C,in} - m_{C \text{ in } CO_2,out} - m_{C \text{ in } CO,out}}{m_{C,in}} \quad (1)$$

*where  $m_{C,in}$  is the mass of total carbon supplied,  $m_{C \text{ in } CO_2,out}$  the mass of carbon in unused  $CO_2$ , and  $m_{C \text{ in } CO,out}$  the mass of carbon in unused  $CO$  in the process.* The carbon efficiency is 94% considering liquid and wax hydrocarbons as the final products. Only 32% of the  $H_2$  produced by electrolysis is stored in the FT products (Fig. 11a). The rest of  $H_2$  is contained in the water formed in the rWGS/CPO and FT steps. Each molecule of  $CO_2$  requires two molecules of  $H_2$  to get rid of the oxygen atoms. Thus, the maximum percentage of  $H_2$  that could be stored in the product would be 33.3%. The hydrogen losses are due to the extra oxygen added for the CPO reactions and the  $H_2$  purged with the rest of purged gases. For that reason, approximately two-thirds of the  $H_2$  actually end up forming water. However, the overall energy efficiency of the Power-to-X plant is 50% considering all the FT products, and thus, over half of the electrical energy harvested by the PV power plant would end up in the FT products. The energy loss due to CPO reactions is approx. 5% of the total energy input. The overall energy efficiency reduces to 47% when only FT oil and wax are considered as final products. *The overall energy efficiency of the PtX plant is calculated from*

$$\eta_E = \frac{E_{FT \text{ oil}} + E_{FT \text{ wax}}}{E_{\text{electrolyzer}} + E_{\text{DAC}} + E_{\text{synthesis}}} \quad (2)$$

*where  $E_{FT \text{ oil}}$  is the chemical energy in the FT oil products,  $E_{FT \text{ wax}}$  the chem-*

ical energy in the FT wax products,  $E_{electrolyzer}$  the electrical energy consumption of the PEM electrolyzer system,  $E_{DAC}$  the electrical energy consumption of the DAC, and  $E_{synthesis}$  the electrical energy consumption of the two-step synthesis.

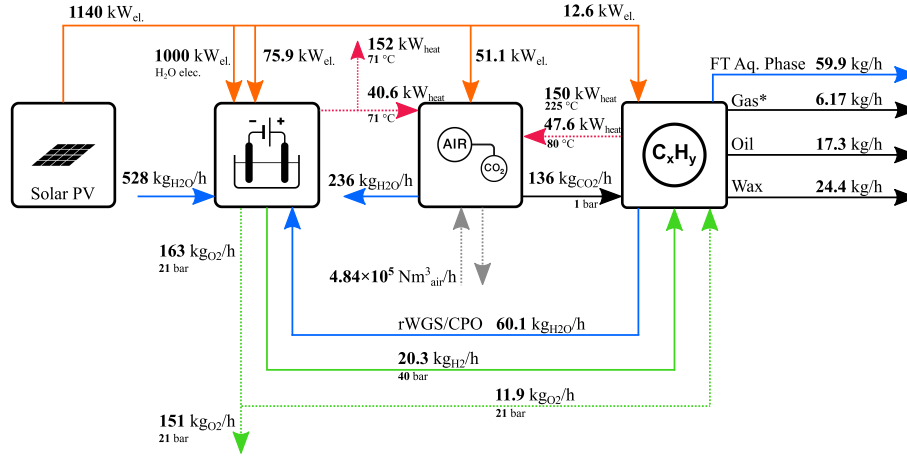


Figure 10: Simplified diagram of the theoretical Power-to-X plant including mass and energy flow streams. \*Purged gas containing unreacted  $H_2$ ,  $CO$ , and  $CO_2$ .

Table 5: Technical specification of each unit in the theoretical Power-to-X plant.

	DAC unit	Water electrolysis unit	Synthesis unit
CO <sub>2</sub> production	136 kg h <sup>-1</sup>	H <sub>2</sub> production	20.3 kg h <sup>-1</sup>
Air flow	4.85 × 10 <sup>5</sup> N m <sup>3</sup> h <sup>-1</sup>	O <sub>2</sub> production	163 kg h <sup>-1</sup>
Blower el. power	51 kW	Water consumption	589 kg h <sup>-1</sup>
Heat power requirement	238 kW	Nominal stack power	1 MW
Type of adsorbent	<i>Amine-based ads. into monoliths</i>	Heat power prod.	193 kW
Operating temp.	ambient to 100 °C	Operating temp.	71 °C
Water prod.	236 kg h <sup>-1</sup>	H <sub>2</sub> & O <sub>2</sub> pressure	20 bar
			Hot trap temp.
			170 °C
			Cold trap temp.
			5 °C
			Purged gas
			6.2 kg h <sup>-1</sup>
			FT oil production
			17 kg h <sup>-1</sup>
			FT wax production
			24 kg h <sup>-1</sup>
			FT aq. phase
			60 kg h <sup>-1</sup>
			rWGS/CPOx water prod.
			60 kg h <sup>-1</sup>
			Recycle compressor
			0.32 kW

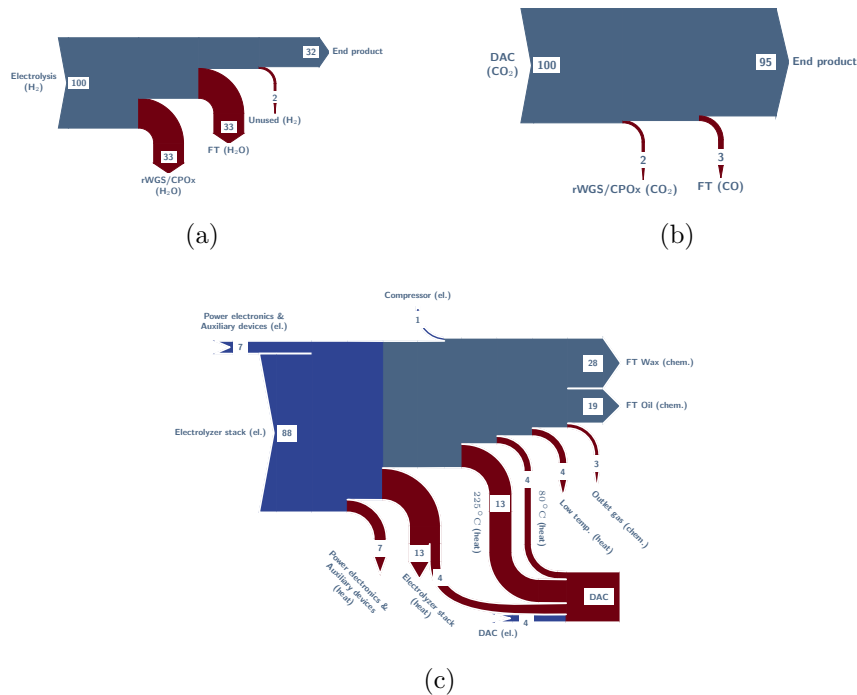


Figure 11: *Sankey diagrams for the overall mass and energy balances of the theoretical Power-to-X plant with 1 MW electrolyzer stack input power. (a) Hydrogen mass balance (% of  $20.3 \text{ kg h}^{-1}$ ). (b) Carbon mass balance (% of  $37.1 \text{ kg h}^{-1}$ ). (c) Energy balance (% of  $1140 \text{ kW}$ ).*

The total average electrical power consumption of the theoretical Power-to-X plant is about 1.14 MW. This electric power is mainly used for electrolysis (1 MW) but also for power electronics (losses) and other auxiliary devices of the  $\text{H}_2$  production unit (76 kW), for the air blowers of the DAC unit (51 kW), and for the compressors of the synthesis unit (12.6 kW). Thus, the power for running the air blowers for the DAC represents less than the 3% of the total energy consumption of the plant. The synthesis unit also includes a two-stage compressor to increase the pressure of the  $\text{CO}_2$  from the

DAC from atmospheric to 20 bar. Considering all these power consumptions, the annual energy consumption of the plant is 9 GW h. The annual solar PV plant production exceeds 2000 kWh/kW<sub>p</sub> in the locations in the world where the annual solar radiation is at highest [51]. Under this assumption and assuming that this plant would be powered only by solar energy, the estimated solar PV panel area needed for this theoretical plant would be 2.6 ha. If the plant is driven solely on solar power, a battery energy storage is needed to compensate for variation in daily radiation. If the plant is constantly consuming the nominal power, the battery energy storage capacity should be in the range of 13 MW h. However, by optimizing the plant for variable energy production by adding a hydrogen intermediate storage, overrating the water electrolyzer, and applying an intelligent plant control, the energy storage capacity could be significantly decreased. Further dynamic operation studies and process optimization are required to optimally dimension the battery and intermediate gas storages.

## 5. Conclusion

The production of carbon neutral fuels based on renewable energy was demonstrated in the SOLETAIR pilot in Finland in 2017. Electricity from a solar PV power plant and the local electricity grid was used for hydrogen production with water electrolysis, direct air capture of CO<sub>2</sub>, and two-step synthesis. Fischer-Tropsch synthesis was applied to produce gas, liquid, and solid (wax) hydrocarbons including co-feeding of H<sub>2</sub> and CO from a gas container. Overall, the system achieved a production of 6.2 kg per day of combined FT oil and wax. The system was operated for about 300 h in four

test campaigns. The total CO<sub>2</sub> and CO conversions were about 38% and 60.3%, respectively, owing to the conversion limitations from the rWGS and FT reactors. Recirculation of unreacted gases into the process would be required to significantly increase the overall carbon utilization. The energy requirement of the DAC was estimated as 26.4 kWhkg<sub>CO<sub>2</sub></sub><sup>-1</sup>, 57.8% of which was the required thermal energy.

A theoretical Power-to-X plant is presented. This plant uses only solar PV electricity, water, and CO<sub>2</sub> from ambient air as the feedstock. All the heat requirement of the DAC unit is supplied by the synthesis and water electrolysis units. The water requirement of the electrolyzer is partly covered by the water condensed after the first step of the synthesis. The carbon efficiency of the plant is 94% considering liquid and wax hydrocarbons as final products. The rest of carbon is lost as a consequence of the purging of the effluent gases in the recirculation loop of the synthesis unit. Although two-thirds of the hydrogen ends up forming water again, half of the energy carried by the hydrogen ends up in the FT products. The overall energy efficiency of the theoretical Power-to-X plant is 47% considering liquid and wax hydrocarbons as final products.

Future studies include measurement and weather forecast based DAC process control and system integration of Power-to-X systems into office buildings. Intelligent control of Power-to-X systems requires studying the dynamic behavior of the Power-to-X system units and the required energy and gas storages allowing off-grid operation.

## **Acknowledgements**

TEKES is acknowledged for the main financial support of the SOLETAIR project (soletair.fi). The project partners are also thanked for their financial and in-kind contributions. The SOLETAIR project concept was developed from the work carried out in the Neo-Carbon Energy project (neocarbonenergy.fi).

All the experimental work was performed on the premises of Lappeenranta University of Technology partly thanks to the work of its personnel and resources. Harri Nieminen (LUT) and Tamer Alhalabi (VTT) are thanked for their work during the preparation and operation of the pilot plant. Other project personnel are also thanked for their work in other tasks related to the pilot plant, special thanks being reserved for Johanna Kihlmann (VTT) and Dr. Pasi Vainikka (VTT).

## References

- [1] S. Fuss, J. G. Canadell, G. P. Peters, M. Tavoni, R. M. Andrew, P. Ciais, R. B. Jackson, C. D. Jones, F. Kraxner, N. Nakicenovic, C. Le Quéré, M. R. Raupach, A. Sharifi, P. Smith, Y. Yamagata, Betting on negative emissions, *Nature Climate Change* 4 (10) (2014) 850–853. doi:10.1038/nclimate2392.
- [2] G. Plessmann, M. Erdmann, M. Hlusiak, C. Breyer, Global energy storage demand for a 100% renewable electricity supply, *Energy Procedia* 46 (2014) 22–31. doi:10.1016/j.egypro.2014.01.154.
- [3] A. Serdoner, K. Whiriskey, Bellona Europa reality check: The 'Power to Liquids' trap, [Accessed: 11-Jun-2018]. (2017).  
URL [http://network.bellona.org/content/uploads/sites/3/2017/04/Power-to-Liquids\\_BellonaEuropa-1.pdf](http://network.bellona.org/content/uploads/sites/3/2017/04/Power-to-Liquids_BellonaEuropa-1.pdf)
- [4] D. W. Keith, G. Holmes, D. S. Angelo, K. Heidel, A process for capturing CO<sub>2</sub> from the atmosphere, *Joule* (Early access) (2018) 1–22. doi:10.1016/j.joule.2018.05.006.
- [5] J. C. Minx, W. F. Lamb, M. W. Callaghan, S. Fuss, J. Hilaire, F. Creutzig, T. Amann, T. Beringer, W. de Oliveira Garcia, J. Hartmann, T. Khanna, D. Lenzi, G. Luderer, G. F. Nemet, J. Rogelj, P. Smith, J. L. V. Vicente, J. Wilcox, M. del Mar Zamora Dominguez, Negative emissions—Part 1: Research landscape and synthesis, *Environmental Research Letters* 13 (6) (2018) 063001.

- [6] EEA, Analysis of key trends and drivers in greenhouse gas emissions in the EU between 1990 and 2014 (2016).
- [7] J. Wilcox, P. C. Psarras, S. Liguori, Assessment of reasonable opportunities for direct air capture, *Environmental Research Letters* 12 (6) (2017) 065001. doi:10.1088/1748-9326/aa6de5.
- [8] J. Wilcox, *Carbon Capture*, Springer, 2012. doi:10.1007/978-1-4614-2215-0.  
URL <https://www.springer.com/gp/book/9781461422143>
- [9] M. Lehner, R. Tichler, H. Steinmüller, M. Koppe, *Power-to-gas: technology and business models*, Springer International Publishing, New York, 2014.
- [10] Audi MediaCenter, [Accessed: 11-Jun-2018].  
URL <https://www.audi-mediacenter.com/de/brennstoffzelle-audi-h-tron-242>
- [11] CRI, World's largest CO<sub>2</sub> methanol plant, [Accessed: 18-Jun-2018]. (2018).  
URL <http://carbonrecycling.is/george-olah/>
- [12] Sunfire, First commercial plant for the production of blue crude planned in Norway, [Accessed: 18-Jun-2018]. (2017).  
URL <https://www.sunfire.de/en/company/press/detail/first-commercial-plant-for-the-production-of-blue-crude-planned-in-norway>

- [13] B. Decourt, B. Lajoie, R. Debarre, O. Soupa, The hydrogen-based energy conversion FactBook, The SBC Energy Institute, 2014.
- [14] R. E. Clarke, S. Giddey, F. T. Ciacchi, S. P. S. Badwal, B. Paul, J. Andrews, Direct coupling of an electrolyser to a solar PV system for generating hydrogen, *Int. J. Hydrogen Energy* 34 (6) (2009) 2531–2542. doi:10.1016/j.ijhydene.2009.01.053.
- [15] P. Schmidt, W. Zittel, W. Weindorf, T. Raksha, Renewables in Transport 2050 — Empowering a sustainable mobility future with zero emission fuels from renewable electricity, Final Report 1086, FVV (2016). doi:10.1007/978-3-658-13255-2.
- [16] L. J. Murphy, K. N. Robertson, R. A. Kemp, H. M. Tuononen, J. A. C. Clyburne, Structurally simple complexes of CO<sub>2</sub>, *Chem. Commun.* 51 (2015) 3942–3956. doi:10.1039/C4CC08510H.
- [17] J. Yu, S. S. C. Chuang, The role of water in CO<sub>2</sub> capture by amine, *Industrial & Engineering Chemistry Research* 56 (21) (2017) 6337–6347. doi:10.1021/acs.iecr.7b00715.
- [18] H. A. Patel, J. Byun, C. T. Yavuz, Carbon dioxide capture adsorbents: Chemistry and methods, *ChemSusChem* 10 (7) 1303–1317. doi:10.1002/cssc.201601545.
- [19] L. Zhang, X. Wang, M. Fujii, L. Yang, C. Song, CO<sub>2</sub> capture over molecular basket sorbents: Effects of SiO<sub>2</sub> supports and PEG additive, *Journal of Energy Chemistry* 26 (5) (2017) 1030–1038. doi:https://doi.org/10.1016/j.jechem.2017.09.002.

- [20] S. Choi, J. H. Drese, P. M. Eisenberger, C. W. Jones, Application of amine-tethered solid sorbents for direct CO<sub>2</sub> capture from the ambient air, *Environmental Science & Technology* 45 (6) (2011) 2420–2427. doi:10.1021/es102797w.
- [21] Y. Kuwahara, D.-Y. Kang, J. R. Copeland, P. Bollini, C. Sievers, T. Kamegawa, H. Yamashita, C. W. Jones, Enhanced CO<sub>2</sub> adsorption over polymeric amines supported on heteroatom-incorporated SBA-15 silica: Impact of heteroatom type and loading on sorbent structure and adsorption performance, *Chemistry — A European Journal* 18 (52) 16649–16664. doi:10.1002/chem.201203144.
- [22] W. Chaikittisilp, H. J. Kim, C. W. Jones, Mesoporous alumina-supported amines as potential steam-stable adsorbents for capturing CO<sub>2</sub> from simulated flue gas and ambient air, *Energy & Fuels* 25 (11) (2011) 5528–5537. doi:10.1021/ef201224v.
- [23] A. Goeppert, S. Meth, G. K. S. Prakash, G. A. Olah, Nanostructured silica as a support for regenerable high-capacity organoamine-based CO<sub>2</sub> sorbents, *Energy Environ. Sci.* 3 (2010) 1949–1960. doi:10.1039/C0EE00136H.
- [24] X. Wang, X. Ma, V. Schwartz, J. C. Clark, S. H. Overbury, S. Zhao, X. Xu, C. Song, A solid molecular basket sorbent for CO<sub>2</sub> capture from gas streams with low CO<sub>2</sub> concentration under ambient conditions, *Phys. Chem. Chem. Phys.* 14 (2012) 1485–1492. doi:10.1039/C1CP23366A.
- [25] M. E. Potter, K. M. Cho, J. J. Lee, C. W. Jones, Role of alumina ba-

- sicity in CO<sub>2</sub> uptake in 3-aminopropylsilyl-grafted alumina adsorbents, *ChemSusChem* 10 (10) 2192–2201. doi:10.1002/cssc.201700115.
- [26] A. Wagner, B. Steen, G. Johansson, E. Zanghellini, P. Jacobsson, P. Johansson, Carbon dioxide capture from ambient air using amine-grafted mesoporous adsorbents, *International Journal of Spectroscopy* 2013 (2013) 1–8. doi:10.1155/2013/690186.
- [27] L. He, M. Fan, B. Dutcher, S. Cui, X. dong Shen, Y. Kong, A. G. Russell, P. McCurdy, Dynamic separation of ultradilute CO<sub>2</sub> with a nanoporous amine-based sorbent, *Chemical Engineering Journal* 189–190 (2012) 13–23. doi:https://doi.org/10.1016/j.cej.2012.02.013.
- [28] D. M. Pacheco, J. R. Johnson, W. J. Koros, Aminosilane-functionalized cellulosic polymer for increased carbon dioxide sorption, *Industrial & Engineering Chemistry Research* 51 (1) (2012) 503–514. doi:10.1021/ie2020685.
- [29] C. Gebald, J. A. Wurzbacher, P. Tingaut, T. Zimmermann, A. Steinfeld, Amine-based nanofibrillated cellulose as adsorbent for CO<sub>2</sub> capture from air, *Environmental Science & Technology* 45 (20) (2011) 9101–9108. doi:10.1021/es202223p.
- [30] W. R. Lee, S. Y. Hwang, D. W. Ryu, K. S. Lim, S. S. Han, D. Moon, J. Choi, C. S. Hong, Diamine-functionalized metalorganic framework: exceptionally high CO<sub>2</sub> capacities from ambient air and flue gas, ultrafast CO<sub>2</sub> uptake rate, and adsorption mechanism, *Energy Environ. Sci.* 7 (2014) 744–751. doi:10.1039/C3EE42328J.

- [31] A. Ursúa, P. Sanchis, Static-dynamic modelling of the electrical behaviour of a commercial advanced alkaline water electrolyser, *Int. J. Hydrogen Energy* 37 (24) (2012) 18598–18614. doi:10.1016/j.ijhydene.2012.09.125.
- [32] Ø. Ulleberg, Modeling of advanced alkaline electrolyzers: A system simulation approach, *Int. J. Hydrogen Energy* 28 (1) (2003) 21–33. doi:10.1016/S0360-3199(02)00033-2.
- [33] M. Carmo, D. Fritz, J. Mergel, D. Stolten, A comprehensive review on PEM water electrolysis, *Int. J. Hydrogen Energy* 38 (12) (2013) 4901–4934. doi:10.1016/j.ijhydene.2013.01.151.
- [34] L. Bertuccioli, A. Chan, D. Hart, F. Lehner, B. Madden, E. Standen, Study on development of water electrolysis in the EU, Final report in fuel cells and hydrogen joint undertaking, 2014.
- [35] P. Millet, S. Grigoriev, Chapter 2 — Water electrolysis technologies, in: L. Gandía, G. Arzamendi, P. Diéguez (Eds.), *Renewable Hydrogen Technologies*, Elsevier, Amsterdam, 2013, pp. 19–41. doi:http://dx.doi.org/10.1016/B978-0-444-56352-1.00002-7.  
URL <http://www.sciencedirect.com/science/article/pii/B9780444563521000027>
- [36] Siemens AG, Kick-off for world’s largest electrolysis system in Mainz, [Accessed: 20-Jun-2018]. (2015).  
URL <http://www.siemens.com/press/en/feature/2014/corporate/2014-05-energiepark-mainz.php>

- [37] Hydrogenics Corporation, E.ON inaugurates energy storage facility using Hydrogenics PEM technology, [Accessed: 11-Jun-2018]. (2015).  
URL <https://globenewswire.com/news-release/2015/10/15/776393/10152542/en/E-ON-Inaugurates-Energy-Storage-Facility-Using-Hydrogenics-PEM-Technology.html>
- [38] M. Hillestad, Modeling the Fischer-Tropsch product distribution and model implementation, *Chemical Product and Process Modeling* 10 (3) (2015) 147–159. doi:10.1515/cppm-2014-0031.
- [39] P. Kaiser, R. B. Unde, C. Kern, A. Jess, Production of liquid hydrocarbons with CO<sub>2</sub> as carbon source based on reverse water-gas shift and Fischer-Tropsch synthesis, *Chemie Ingenieur Technik* 85 (4) (2013) 489–499. doi:10.1002/cite.201200179.
- [40] F. Vidal Vázquez, P. Pfeifer, J. Lehtonen, P. Piermartini, P. Simell, V. Alopaeus, Catalyst screening and kinetic modeling for CO production by high pressure and temperature reverse water gas shift for Fischer-Tropsch applications, *Industrial and Engineering Chemistry Research* 56 (45) (2017) 13262–13272. doi:10.1021/acs.iecr.7b01606.
- [41] J. Xu, G. F. Froment, Methane steam reforming, methanation and water-gas shift: I. Intrinsic kinetics, *AIChE Journal* 35 (1) (1989) 88–96. doi:10.1002/aic.690350109.
- [42] A. Kosonen, J. Ahola, C. Breyer, A. Albó, Large scale solar power plant in Nordic conditions, in: 2014 16th European Con-

- ference on Power Electronics and Applications, 2014, pp. 1–10. doi:10.1109/EPE.2014.6911030.
- [43] J. Koponen, A. Kosonen, V. Ruuskanen, K. Huoman, M. Niemelä, J. Ahola, Control and energy efficiency of PEM water electrolyzers in renewable energy systems, *Int. J. of Hydrogen Energy* 42 (50) (2017) 29648–29660.
- [44] A. Moro, L. Lonza, Electricity carbon intensity in European member states: Impacts on GHG emissions of electric vehicles, *Transportation Research Part D: Transport and Environment*-doi:https://doi.org/10.1016/j.trd.2017.07.012.
- [45] J. Elfving, C. Bajamundi, J. Kauppinen, T. Sainio, Modelling of equilibrium working capacity of PSA, TSA and TVSA processes for CO<sub>2</sub> adsorption under direct air capture conditions, *Journal of CO<sub>2</sub> Utilization* 22 (2017) 270–277. doi:10.1016/j.jcou.2017.10.010.
- [46] J. Elfving, C. Bajamundi, J. Kauppinen, Characterization and performance of direct air capture sorbent, *Energy Procedia* 114 (2017) 6087–6101, 13th International Conference on Greenhouse Gas Control Technologies, GHGT-13, 14–18 November 2016, Lausanne, Switzerland. doi:https://doi.org/10.1016/j.egypro.2017.03.1746.
- [47] Climeworks, Capturing CO<sub>2</sub> from air, [Accessed: 12-Jun-2018]. (2018). URL <http://www.climeworks.com>
- [48] B. H. Davis, Fischer-Tropsch synthesis: Overview of reactor develop-

- ment and future potentialities, *Topics in Catalysis* 32 (3-4) (2005) 143–168. doi:10.1007/s11244-005-2886-5.
- [49] M. Ostadi, E. Rytter, M. Hillestad, Evaluation of kinetic models for Fischer-Tropsch cobalt catalysts in a plug flow reactor, *Chemical Engineering Research and Design* 114 (3) (2016) 236–246. doi:10.1016/j.cherd.2016.08.026.
- [50] J. R. Couper, W. R. Penney, J. R. Fair, S. M. Walas, *Chemical Process Equipment: Selection and Design*, 2nd Edition, Elsevier Inc., 2010.  
URL <https://www.sciencedirect.com/science/book/9780123969590#book-info>
- [51] T. W. B. Group, *Global Solar Atlas*, [Accessed: 18-Jun-2018]. (2018).  
URL <http://www.globalsolaratlas.info/>